Superoxide Dismutases maintain niche homeostasis in stem cell populations

Olivia Majhi[1], Aishwarya Chhatre[1,2], Tanvi Chaudhary[1] and Devanjan Sinha[1#]

[1]Department of Zoology, Institute of Science, Banaras Hindu University, Varanasi, Uttar Pradesh, India

[2]Present address: Biological Research Centre, Institute of Genetics, Eötvös Loránd Research Network (ELKH), Szeged, Hungary

[#]To whom correspondence should be addressed:

Address for correspondence:
Dr. Devanjan Sinha,
Department of Zoology,
Institute of Science,
Banaras Hindu University,
Varanasi – 221005,
Uttar Pradesh, India
India
Email: devanjan@bhu.ac.in

Abstract

Reactive oxygen species (ROS), predominantly derived from mitochondrial respiratory complexes, have emerged as key molecules influencing cell fate decisions like maintenance and differentiation. These redox-dependent events are mainly considered to be cell intrinsic in nature, on the contrary our observations indicate involvement of these oxygen-derived entities as intercellular communicating agents. In *Drosophila* male germline, Germline Stem Cells (GSCs) and neighbouring Cyst Stem Cells (CySCs) maintain differential redox thresholds where CySC have higher redox-state compared to the adjacent GSCs. Disruption of the redox equilibrium between the two adjoining stem cell populations by depleting Superoxide Dismutases (SODs) especially Sod1 results in deregulated niche architecture and loss of GSCs, which was mainly attributed to loss of contact-based receptions and uncontrolled CySC proliferation due to ROS-mediated activation of self-renewing signals. Our observations hint towards the crucial role of differential redox states where CySCs containing higher ROS function not only as a source of their own maintenance cues but also serve as non-autonomous redox moderators of GSCs. Our findings underscore the complexity of niche homeostasis and predicate the importance of intercellular redox communication in understanding stem cell microenvironments.

52 **Introduction**

53 Studies from the past few decades have shown the apparent role of ROS in influencing
54 various biological processes[1-3]. ROS are usually produced in specific cellular
55 compartments close to their target molecules to regulate important signaling
56 pathways.[4]. Mitochondria, a major source of oxidant species[5,6], localize dynamically
57 towards nucleus, effecting oxidation induced reshaping of gene expression profiles[7].
58 Localized ROS production are contributed by NADH oxidases distributed across
59 different cellular regions[8]. Intracellular hydrogen peroxide gradients maintained by
60 thioredoxin system allow intercompartmental exchanges among endoplasmic
61 reticulum (ER), mitochondria and peroxisomes[9-11].

62 The process of redox relays is conserved and plays a fundamental role in self-renewal
63 and differentiation of stem cell populations[12]. Stem cells whether embryonic or adult
64 maintain a low redox profile, characterized by subdued mitochondrial respiration[13-17].
65 Levels of ROS are tightly regulated and elevated amounts promote early differentiation
66 and atypical stem cell behaviour[18]. However, leading evidences suggest that many
67 transcription factors require oxidative environment for the maintenance of pluripotent
68 states. For instance, physiological ROS levels play a crucial role in genome
69 maintenance of embryonic stem cells[13]. Multipotent hematopoietic progenitors,
70 intestinal stem cells [19] and neural stem cells require relatively high baseline redox for
71 their maintenance[14,16,20]. Suppression of Nox system or mitochondrial ROS
72 compromises the maintenance of these self-renewing populations and promote their
73 differentiation or death[18]. These evidences point towards the essentiality of a well-
74 tuned redox state for balancing the pluripotent and differentiated states. However, how
75 stem cells regulate their redox potential by possessing a restrained oxidant system is
76 not very clear.

77 We addressed this fundamental question in two-stem cell population-based niche
78 architecture in *Drosophila* testis. The testicular stem cell niche is composed of a
79 central cluster of somatic cells called the hub which contacts eight to eleven GSCs
80 arranged in a round array[21,22]. A pair of cyst stem cells (CySCs) enclose each GSC
81 and make their independent connections with the hub and GSCs via adherens
82 junctions[23-28]. The hub cells secrete self-renewal factors essential for both GSCs and
83 CySCs maintenance involving signalling cascades like Jak-Stat signalling[29,30], BMP

84 (Bone Morphogenetic Signalling)[31], Hedgehog signalling[32]. The hub and CySCs
85 produce BMPs which repress GSC differentiation by suppressing transcription of bag-
86 of-marbles (Bam)[31,33]. Concerted asymmetric division of both GSC and CySC is
87 essential for proper cyst formation[34]. A developing cyst contains a dividing and
88 differentiating gonialblast encircled by cyst cells that provide nourishment to
89 developing spermatids[35,36]. However, the maintenance of GSCs in the spatially
90 controlled microenvironment is still not very clear.

91 We found the existence of a balanced differential redox state between GSC and CySC
92 essential for niche homeostasis. CySCs by virtue of their higher redox threshold and
93 more clustered mitochondria generate an intercellular redox state that affects the
94 physiological ROS levels in GSCs. Alterations in CySC redox state resulted in self-
95 renewal and differentiation propensities of the GSCs. Intercellular redox-imbalance
96 induced niche disequilibrium through precocious differentiation of GSCs and
97 deregulated CySC proliferation, due to activation of pro-proliferative transductions and
98 loss of cell-cell contact signalling. Our results indicate a sophisticated interplay in these
99 two stem cell populations where a higher redox state in CySCs not only supports their
100 self-renewing processes but also non-autonomously promotes the maintenance of
101 GSCs.

102

103 **Results**

104 **CySCs maintain higher differential ROS in comparison to adjacent GSCs**

105 The apical region of the *Drosophila* testis incorporates a cluster of differentiated cells,
106 the hub surrounded by GSCs in a rosette arrangement with each GSC being enclosed
107 by two CySCs (Fig. 1A). Immunostaining ATP5A subunit of mitochondrial ATPase and
108 marking cell boundary by discs-large (Dlg) indicated different mitochondria
109 morphology (Fig. 1G) and distribution among these two stem cell populations. In wild
110 type adult testis, we observed fragmented mitochondria in Vasa^{+} GSCs as compared
111 to a fused organization in CySCs (Fig. 1B#, C, D, and S1B-B'')**.** The number of
112 mitochondria per cell was higher in CySC (Fig 1F) and had a more elongated shape
113 (reduced circularity) than the GSCs (Fig 1G). The ATP5A labelling overlapped with
114 *TFAM-GFP*, a mitochondrial transcription factor[37], further confirming the patterning

115 observed between these two stem cell populations (Fig. S1A). Mitochondria
116 localization and dispersion pattern in GSCs and CySCs, corresponded with the
117 intensity variance of the ROS reporter line *gstD1-GFP*[38] at the niche (Fig. 1L and
118 S1C'''). CySCs exhibited a higher baseline level of ROS compared to GSCs (Fig.1R).

119 To affirm the role of CySC in influencing GSC redox state, we asked if disrupting the
120 dismutases in CySCs would influence the redox state of GSCs. We depleted the
121 expression of superoxide dismutase 1 (Sod1) in the hub, CySCs and early
122 differentiating cyst cells (CCs) using *Tj-Gal4*[39] driver (*Tj>Sod1i*) that resulted in a net
123 increase in *gstD1*-GFP intensity (Fig. 1Q, D'' and S1E). The elevated redox state in
124 CySCs led to a corresponding increase in ROS levels in adjacent GSCs, as evidenced
125 by the increased *gstD1*-GFP intensity (Fig.1Q and S) and an overall rise in superoxide
126 levels, confirmed through DHE fluorescence analysis (Fig.S1F). This suggests a
127 potential redox crosstalk between these stem cell populations, where the redox state
128 of CySCs influences the oxidative status of neighbouring GSCs.

129

130 **Balanced CySC redox profile is crucial for its proliferation and GSC**
131 **maintenance**

132 Alongside the differential redox profile, we observed that elevated ROS levels in
133 *Tj>Sod1i* had a striking effect on the increase of DAPI$^+$ nuclei at the testis tip (Fig.
134 2A''). This overcrowding was attributed to both an increase in the number of Tj$^+$ CySCs
135 and early differentiating CCs, as well as their positional shift (Fig. 2A', B', and E). To
136 further validate these findings, we used an alternative driver line, *C-587-Gal4*, which
137 specifically drives expression in CySCs and CCs. This also resulted in an increase in
138 the total number of Tj$^+$ cells (Fig. S1H', and M) although to a lesser extent than *Tj-*
139 *Gal4*, suggesting that signals from the hub may also partially influence CySC
140 proliferation. Given the stronger phenotypic effect observed with *Tj-Gal4*, we
141 proceeded with this driver line for subsequent experiments.

142 The enhancement in the number of CySCs was also reflected by ~2-fold change in
143 Zfh1$^+$ cells (Fig. 2F, S2R-S). However, Vasa$^+$ cells flanking the hub (GSCs) showed a
144 substantial reduction in number (Fig. 2C''-D'' and G). This decline was further validated
145 by western blot analysis, which revealed lower overall detectable levels of Vasa

146 protein, indicating a potential impact of the altered redox state on GSC maintenance
147 and stability. (Fig. S2N). *C-587-Gal4* also showed a reduction in the number of
148 neighbouring GSCs (Fig.S1N). The observations were further verified using *Sod1i*
149 localized in different chromosome to avoid any chromosome or balancer-based
150 biasness (Fig. S1I-L and O-P). However, the phenotypic effect of higher ROS was
151 limited to its origin in CySCs only because ablation of GSC redox status did not cause
152 any marked change in niche composition. *Nos-Gal4* driven knock-down of Sod1 in
153 GSCs did not result in significant change in CySC number (Fig. S2A', B' and E) but
154 effected a considerable reduction on Vasa^{+} cells (Fig. S2C', D' and F), aligning with
155 previous observations[17]. Although Sod1 is the predominant enzyme which also
156 localizes in the intermembrane space of mitochondria, we observed a similar result
157 upon depleting the matrix localized Sod2 in both GSCs and CySCs (Fig. S2G-M),
158 indicating the involvement of mitochondrial ROS for the observed cellular phenotypes.

159 To confirm the active proliferation of cells and rule out the possibility of arrested
160 growth, we utilized fly-Fluorescent Ubiquitination-based Cell Cycle Indicator (FUCCI)
161 system[40] which comprises of two reporter constructs marking G1/S transition (green),
162 S (red) and G2/early mitosis (yellow) (Fig. 2H). Testes from *Tj>Sod1i* exhibited an
163 approximately two-fold increase in cell number across all stages of the cell cycle (Fig.
164 S2O). However, the percentage of cells in each phase remained unchanged (Fig 2I),
165 indicating that the observed increase in different phases is a consequence of more
166 cells entering proliferation rather than alterations in the duration of different cell-cycle
167 stages. The enhanced number of dividing cells was contributed mainly by progressive
168 division of CySCs, showing >2-fold difference in the accumulation of Zfh1^{+} nuclei in S
169 and G2/M phases (Fig. 2J, S2RV-VII and SV-VII). The number of Zfh1 labelled cells
170 in G1/S transition was also substantially more (Fig. S2RIII and SIII), indicating
171 dysregulated redox ensued an increased mitotic index of CySCs. The enhanced
172 mitotic activity of these proliferating niche cells is further supported by increased
173 phospho-histone H3 (PH3) incorporation, indicating a higher mitotic frequency
174 compared to the control (Fig. S2T, U), along with elevated cyclin D expression (Fig.
175 S2Q). Downregulation of Sod1 in GSCs through *Nos-Gal4* demonstrated no significant
176 change in G1/S, S and G2/M phase numbers, confirming our previous observation
177 that altering ROS levels in GSCs does not have any non-autonomous effect on CySCs
178 (Fig. S2P).

179

180 **CySC induced ROS couples precocious differentiation of stem cell lineages**

181 Since in *Tj>Sod1i* testes, the increased number of Tj$^+$ cells, marking CySCs and early
182 differentiating cells, exceeded the number of CySC-specific Zfh1$^+$ cells (Fig. 2J and
183 S2O), we checked for parallel enhancement of cellular differentiation using the
184 corresponding marker, *Eya* (Eyes absent).

185 We found that Eya$^+$ cells clustered towards the hub along with a significant increase
186 in their number in Sod1 depleted CySCs (Fig. 3A, B and D). This increased number of
187 Eya$^+$ cells does not suggest that these differentiating cells are proliferative. Instead,
188 we propose that the knockdown of Sod1 may alter the timing or regulation of cyst cell
189 differentiation, leading to an accumulation of Eya$^+$ cells near the niche. The supposed
190 premature expression of Eya resulted in a population of differentiating cyst precursor
191 cells co-expressing Eya-Zfh1 (Fig. 3A'', B'' and D). This population was found to be
192 deviating from the normal partitioning of wild-type representative populations (Fig. 3C).
193 In contrast, depletion of *Sod1i* in the germline lineage using *Nos-Gal4* did not result in
194 a similar phenotypic arrangement (Fig. S3A-D). These findings suggest that alterations
195 in the redox state of GSCs can impact their numbers, even when the changes are
196 induced non-autonomously through CySCs.

197 Together with reduction in Vasa$^+$ GSCs shown earlier (Fig. 2G), we also detected
198 gonialblast expressing differentiation-promoting factor Bam to be much closer to the
199 hub in *Tj>Sod1i* testes (Fig. 3E'' and F''). The mean distance between the hub and
200 Bam$^+$ cells was found to be shortened by ~7 microns (Fig 3G). The relative
201 advancement of spermatogonial differentiation towards the hub was also ascertained
202 by tracking the transformation of GSC-specific spectrosome into branched fusomes
203 connecting the multi-cell gonialblast (Fig. 1A). The branching fusomes were found
204 more proximal to hub than controls (Fig. 3H, I'' and J''), along with parallel reduction
205 in number of spectrosomes, implying a decline in early-stage germ cells (Fig. S3F).
206 This loss could possibly be attributed to loss of intercellular contacts, particularly with
207 hub cells (Fig. 2C# and D#). The observation corroborated with decreased expression
208 pattern of E-cadherin in *Tj>Sod1i* flanking the hub and GSCs (Fig. 3K- M) and could
209 be one of the reasons for GSCs dissociation and differentiation (Fig. 2D#),
210 Disengagement of GSCs from the hub caused reduction in Socs36E and Ptp61F

211 transcripts that act as drivers of E-cadherin expression (Fig. 3N and O). These results
212 suggest that disruption of intercellular redox gradient affected the premature
213 differentiation of stem cells in the niche.

214

215 **Disrupted niche architecture compromises GSC-CySC communication**

216 GSCs and CySCs intercommunicate through several factors such as EGFR, PI3K/Tor,
217 Notch[41] to support CySC maintenance[42]. EGF ligands secreted by spermatogonia
218 maintain differences in cell polarity and segregates self-renewing from differentiating
219 populations[43]. *Tj>Sod1i* cells showed lower levels of cell-polarity marker Dlg (Fig. 4A",
220 B" and E), that expanded more into the differentiated zone (Fig. S4A). Since, Dlg
221 expression is dependent on EGFR[44], impairment in its reception was reflected in net
222 reduction in pErk levels across sections in *Sod1i* testis (Fig. 4C', D' and F). This
223 reduction in overall Erk levels may be attributed to the loss of cell contact and altered
224 GSC-CySC balance in *Sod1i* testis**,** probably resulting in lower EGF response. The
225 uncontrolled proliferation of cyst cells correlates with increased levels of self-renewal
226 inducers, including the elevated expression of Hedgehog (Hh) pathway components
227 [32] in *Tj>Sod1i* testis. The depletion of Sod1 in CySC resulted in elevated expression
228 of Hh receptor Patched (Ptc) (Fig. 4I, S4V) which extended to regions farther from the
229 hub, overlapping with expanded Tj^+ cells (Fig. 4G and H). Since, Ptc itself is a
230 transcriptional Hh target, its expression in CySCs suggests active Hh signalling[45],
231 further supported by higher levels and a similar pattern of Hh transcriptional effector
232 Cubitus interruptus (Ci) in *Sod1i* testis (Fig. 4M'', N'', J and S4W). Since, Ptc, Ci, and
233 a GPCR-like signal transducer Smoothened (Smo) are all transcriptionally driven by
234 Hh, and Hh itself is regulated by higher levels of Ci[46,47], we expectedly found higher
235 levels of transcripts for these pathway genes (Fig. S4C-F). The overt proliferation of
236 CySCs under high ROS conditions was suppressed by reducing gene dosage using
237 *Hh-RNAi* (Fig. 4L and Fig. S4G-I), which was associated with rescue in the GSC
238 population (Fig. 4K and S4J-L). The levels of Sod1 transcripts under single and Sod1,
239 hh double depletion were almost similar (Fig. S4M). To determine whether the
240 changes observed in the germ cell population were a sole consequence of *Sod1*
241 knockdown in CySC, we manipulated CySC numbers using *UAS-Ci* and assessed
242 their impact on neighbouring GSCs. Ci overexpression driven by *Tj-Gal4* led to a

243 higher number of Tj$^+$ cells (Fig. S4N, and R'') and a complete loss of Vasa$^+$ GSCs (Fig.
244 S4O, and R'''). However, the effect on CySC and GSC population was less severe
245 when driven by *C-587 Gal4* (Fig.S4N, O, Q''and Q''').

246

247 **Elevating CySC antioxidant defence promotes GSC self-renewal**

248 To further substantiate the role of ROS in coordinating the stem cell populations, we
249 strengthened the cellular defences against oxidants by overexpressing Sod1 in
250 CySCs. We checked the overall ROS level using DHE (Fig. S5I) and monitored the
251 relative GSC/CySC populations. Together with reduction in superoxide levels, we
252 observed an increase in the number of Vasa$^+$ cells (Fig. 5A and S5A''-B''), and a slight
253 reduction in Tj$^+$ cells (Fig. 5B and S5E''-F''). Any morphological anomalies associated
254 with cell-cell adhesion or abnormal cellular dispersion, was not observed (Fig. S5A-B
255 and E-F). Enhancing the levels of Sod1 in GSCs promoted the growth of GSC-like
256 cells (Fig. S5C'', D'' and J) but did not have any prominent effect on CySCs (Fig. S5G'',
257 H'' and K). The increment in Vasa$^+$ GSCs under CySC-induced low redox conditions
258 was also represented by a parallel increase in spectrosome number (Fig. 5C-E). The
259 uptick in GSC number due to scavenging of ROS in CySC, might be a result of delayed
260 differentiation as indicated by displacement of Bam$^+$ zone away from hub; thus,
261 confirming non-cell-autonomous role of CySC ROS in maintaining GSC fate (Fig. 5F-
262 H). The data suggest that reducing redox profile of CySCs differentially affected their
263 own self-renewing propensities along with GSC maintenance and optimum redox state
264 of both the stem-cell populations is controlled by CySCs.

265

266 **Discussion:**

267 ROS is a crucial mediator of stem cell maintenance where these species act as second
268 messengers to induce different post-translational protein modifications thereby,
269 affecting cell fate[48,49]. The effect of ROS is mainly considered to be autocrine in nature,
270 where generation of these oxidative species is usually restricted to specific cellular
271 compartments, ensuring they act close to their targets. Recent studies have reported
272 non-autonomous generation of ROS by NOX enzymes or upon stimulation by growth
273 factors, to play a critical role in regenerative growth[50-52]. However, in either of the

274 cases, the target cell serves as the source and the site of response. Among ROS,
275 hydrogen peroxide (H_2O_2) stands out due to its stability and membrane permeability[53],
276 allowing it to diffuse from its source[54]. Our observations in *Drosophila* testicular stem
277 cell niche suggested a previously unaccounted role of superoxide dismutases in
278 maintaining niche homoeostasis. The redox perturbations affected cyst stem cell
279 dynamics which indirectly influenced the germline. The higher ROS threshold of
280 CySCs maintained the physiological redox state of GSCs. Reduced ROS in GSC was
281 accompanied with its proliferation[55], phenocopied when Sod1 was overexpressed in
282 its neighbours (Fig. 5). However, we feel that net alterations in GSC state were the
283 combinatorial effect of oxidative stress and niche alterations brought about by CySC
284 deregulation.

285 GSCs are anchored to the hub cells via adherens junctions, allowing them to receive
286 crucial maintenance signals[28]. These include Bone Morphogenetic Proteins (BMPs)
287 such as Decapentaplegic (Dpp) and Glass bottom boat (Gbb), which activate the BMP
288 pathway[31] required for GSC self-renewal, and Unpaired (Upd), which triggers the JAK-
289 STAT pathway to promote GSC adhesion to the hub[56]. The suppression of these
290 pathways activates Bam, acting as a switch from transit-amplifying cells to
291 spermatocyte differentiation[57,58]. E-cadherin levels ensure only undifferentiated stem
292 cells persist within the niche, while differentiating GSCs lose the competition for niche
293 occupancy[26]. Elevated ROS in CySC possibly affected STAT phosphorylation through
294 S-glutathionylation[59,60], reducing the levels of STAT-dependent transcripts such as
295 Socs36E[61], Ptp61F and E-cadherin. This depletion compromises GSC adhesion,
296 resulting in detachment from neighboring cells, similar to E-cadherin loss conditions.
297 [56,62-64]. This resulted in compromised GSC-CySC paracrine receptions such as EGFR
298 which play a crucial role in the maintenance of cell-polarity that segregates self-
299 renewing CySC populations from the ones receiving differentiation cues [43,65,66], leading
300 to the accumulation of cells co-expressing both stemness and differentiation markers.
301 In contrast to GSCs, ROS imbalance in CySCs induced accelerated proliferation as
302 well as differentiation due to deregulation of EGFR and Hedgehog pathways.
303 Although, redox modulation of EGFR pathway components has been previously
304 demonstrated[67], in this study we found Hedgehog to be probably susceptible to redox
305 regulation. The redox dependent induction of Hedgehog probably, contributed to
306 enhancement in CySC numbers which partly contributed to depletion of GSCs.

307 However, we do not rule out the possibility of hub cells playing an equivalent role in
308 GSC maintenance, given their parallel effect in suppressing GSC differentiation[30]. *Tj-*
309 *Gal4* depleting Sod1 in both the hub and CySCs, presented a stronger phenotype that
310 CySC specific driver *C587-Gal4*, indicating potential hub contributions. We had also
311 tried using *E-132 Gal4* particularly expressed in the hub to express *Sod1i* lines in hub
312 cells but were challenged by substantial adverse effect on fly viability. While ROS
313 accumulation typically enhances EGFR signaling promoting premature GSC
314 differentiation[68], the loss of EGFR in somatic cells increases the number of GSCs[65]
315 and reduced EGFR activity leads to fewer somatic cells [69]. However, we feel that the
316 response of germline to EGFR modulation is more context-dependent as *Sod1*
317 depletion caused parallel reduction of pErk level and GSC number. We tried an EGFR
318 gain-of-function rescue of CySC depletion but the driven progenies were lethal in the
319 absence of Sod1. We also avoided usage of Gal80 dependent clonal populations to
320 maintain a homogenous genetic background and prevent false readouts due to
321 diffusion of ROS signals in unaltered neighbourhood.

322 The proposed concept of intercellular ROS communication can be of importance in
323 deciphering the biochemical adaptability and plasticity of different niches influencing
324 stem cell fate, ensuring niche size and architecture to prevent stem cell loss and aging.
325 This has been observed in neural stem cells where inflammation-induced quiescence
326 recovers the regenerating capacity of aging brain[70]. In addition to metabolic variations,
327 dependence of the germline on somatic neighbours for its redox state might be one
328 the reasons behind its presumed immortal nature and resistance to aging[71]. The same
329 can also be applied to cancer stem cells, which maintain niche occupancy and resist
330 oxidative stress-induced apoptosis, probably by receiving redox cues from the
331 environment. However, further work is required to elucidate the myriads of driver
332 mechanisms intersecting in the realm of redox regulation that extend beyond the
333 present system into broader translational areas.

334

335

336

Materials and Methods

Fly strains

Fly stocks were maintained and crosses were set at 25°C on normal corn meal and yeast medium unless otherwise indicated. All fly stocks (BL-24493) *UAS SOD1 RNAi*, (BL-32909) *UAS SOD1 RNAi*, (BL-29389) *UAS SOD1 RNAi*, (BL-32983) *UAS SOD2 RNAi*, (BL-24754) *UAS SOD1*, (BL- 32489) *UAS hhRNAi*, (BL- 25751) *UAS Dcr-nos Gal4*, (BL-55122) *UAS-FUCCI*, were obtained from Bloomington Drosophila Stock Centre. *Nos-Gal4*, *Tj-Gal4*, *Tj-Gal4-BamGFP*, *gstD1-GFP*, *TFAM-GFP, UAS-Ci* were kind gift from U. Nongthomba, P. Majumder, K. Ray, B. C. Mandal, Hong Xu, LS Shahidhara labs respectively. Parents were maintained at 25°C, and crosses were set at the same temperature. To ensure optimal Gal4 activity, progenies were shifted to 29°C until eclosion, with aging also conducted at 29°C. Males aged 3–5 days were used for all experiments. The control lines for all experiments are the corresponding Gal4-line crossed with wild type *OregonR*$^{+}$.

Dissection and immunostaining

Anesthetized flies were dissected in 1X Phosphate Buffer Saline (PBS). All incubations were carried out at room temperature (25°C) unless otherwise mentioned. Testes were fixed in 4% paraformaldehyde for 30 minutes, followed by three washes with 0.3% PBTX (PBS + TritonX 100). Post-blocking in 0.5% Bovine Serum Albumin, testis was incubated overnight at 4°C for primary antisera, followed by washing in 0.3% PBTX 3 times 15 minutes each before incubating with secondary antibody. The tissues were counterstained with DAPI (4,6-diamidino-2-phenylindole) for 20 minutes, followed by three washes in 0.3% PBTX for 15 minutes each. For Patched antibody staining, a modified protocol utilizing PIPES-EGTA buffer was used as described[72]. For Eya staining, the tissues were incubated in primary antibody for 2 days. The dpErk was labelled by dissecting fly testes in Schneider's media, followed by fixation in 4% PFA for 30 min, 3x wash in 0.1% PBTX, blocked and incubated in primary antibody overnight; each step supplemented with phosphatase inhibitor cocktail 2 (1:100, Sigma, cat#P5726). Samples were mounted in DABCO anti-fade medium prior imaging.

368 The following primary antibodies were used in the experiments - anti-FasIII (7G10)
369 (1:120, DSHB (Developmental Studies Hybridoma Bank)), anti-Eya (1:50, DSHB),
370 anti-DEcad (DCAD2) (1:50, DSHB), anti-α-Spectrin (3A9) (1:20, DSHB), anti-Ptc
371 (1:50,DSHB) , anti-Ci (1:50, DSHB), anti -Dlg (1:50), anti-βtubulin (1:300, DSHB), anti-
372 pERK (1:100, Cell Signaling (4370)), ATP5A (1:700, Abcam (ab14748)), anti-Tj
373 (1:5000), anti-Vasa (1:4000), anti-Zfh1(1:2000). The primary labelling was detected
374 using appropriate Alexa-Flour tagged secondary antibody (ThermoFisher Scientific).

375 To assess superoxide levels, testes were dissected in Schneider's medium (SM) and
376 immediately incubated in 30 µM Dihydroxyethidium (DHE) at 25 °C in the dark. Testes
377 were washed thrice with SM for 7 minutes each before quantifying the emitted
378 fluorescence using SpectraMax iD5 (Molecular Devices).

379

380 **Quantitative Reverse transcription–PCR**

381 For semi-quantitative RT-PCR and qRT-PCR analyses, total RNA was isolated from
382 testes of 3-5 days old male flies using Qiagen RNA extraction kit. RNA pellets were
383 resuspended in nuclease-free water and quantity of RNA was spectrophotometrically
384 estimated. First-strand cDNA was synthesized from 1-2 µg of total RNA as described
385 earlier. The prepared cDNAs were subjected to real time PCR using forward and
386 reverse primer pairs as listed below, using 5 µl qPCR Master Mix (SYBR Green,
387 ThermoFisher Scientific), 2 pmol/µl of each primer per reaction for 10 µl final volume
388 in ABI 7500 Real time PCR machine. The fold change in expression was calculated
389 through $2^{-\Delta\Delta Ct}$ method. The primers used are listed in Supplementary Table S1.

390

391 **Imaging and image analysis**

392 Confocal imaging was carried out using Zeiss LSM 900 confocal microscope, using
393 appropriate dichroics and filters. Images were further analyzed and processed for
394 brightness and contrast adjustments using ImageJ (Fiji). Mean intensity
395 measurements were carried out using standard Fiji plug-ins,The relative distance from
396 the two reference points in the images was estimated through Inter-edge Distance
397 ImageJ Macro v2.0 from Github. All images were assembled using Adobe Photoshop
398 version 21.2.1.

399 **Quantification of GSCs, CySCs and CCs**

400 For GSC quantification, only cells in direct contact with the hub were considered. While
401 single slices are shown for representation, counting was performed on individual slices
402 of z-stacks using the semi-automated Cell Counter plugin in Fiji for all specified
403 genotypes.

404 For CySC quantification, all Tj-positive and Zfh1-positive cells present in each testis
405 were counted and represented. For cyst cells quantification, only those near the hub
406 were considered, which does not reflect the total number of Eya-positive cells. All
407 quantifications were performed using the Cell Counter plugin in Fiji.

408

409 **Mitochondrial and GstD-GFP quantification:** The mitochondrial analyzer first
410 generates 2D mitochondrial regions of interest (ROIs), followed by the measurement
411 of their total area and circularity. Initially, this is done using a thresholded image of a
412 single slice. For *GstD-GFP* quantification**,** we have manually demarcated the cell,
413 taking Dlg as a reference, and quantified the GFP intensity.

414

415 **Immunoblot Analysis**

416 Protein was extracted from the dissected testes using RIPA buffer as described
417 previously and quantified using Bradford reagent (Biorad). Equivalent concentration of
418 lysate was denatured using 1X Laemelli Buffer with 1 M DTT at 95°C, separated in
419 10% SDS-PAGE and transferred onto PVDF membranes. Membranes were blocked
420 with commercial blocking solution in TBST base before sequential primary antibody
421 incubation with anti-Vasa and anti-β-Tubulin (DSHB, E7). Secondary detection was
422 performed using HRP-tag anti-mouse antibody (GE Amersham).

423

424 **Statistical analyses**

425 The sample sizes carrying adequate statistical power are mentioned in the figure
426 legends. Statistical significance for each experiment was calculated using two-tailed
427 Student's t-test, unless otherwise mentioned, using GraphPad Prism 8 software. The
428 *P* values were calculated through pairwise comparison of the data with wild type or

driver alone and driven RNAi lines. Significance values for sample sizes mentioned in figure legends were represented as *$P < 0.01$, **$P < 0.001$, or ***$P < 0.0001$.

Author contribution

D.S. and O.M conceived the study and designed the experiments. O.M, A.C and T.C performed the experiments. D.S and O.M analyzed the data. D.S, O.M. and A.C. wrote the manuscript.

Acknowledgements

We thank P. Majumder, U. Nongthomba, K. Ray, G. Ratnaparkhi, B. C. Mandal, Hong Xu lab and S. C. Lakhotia for kindly sharing some of the transgenic fly lines. Christian Bökel for sharing experimental protocols. Anti-Tj antibody was a generous gift from Prof. D. Godt, University of Toronto. Anti-Vasa and Anti-Zfh1 were kindly gifted by Prof. R. Lehmann, New York University. We also thank Dr. Bama Charan Mandal for generously sharing his Confocal microscope imaging system and Sudeshna Majumder for preliminary data. We acknowledge BDSC for fly stocks and DSHB for antibodies. This work is supported by Innovative Young Biotechnologist Award by Department of Biotechnology (BT/12/IYBA/2019/01), Early Career Research Award by Science and Engineering Research Board (ECR/2018/000009), BHU-Institute of Eminence grant (R/Dev/IoE/Incentive/2021-22/32452). The authors also acknowledge financial support from DST-INSPIRE fellowship (to O.M.) and UGC-CAS doctoral fellowship (to T.C.).

Declaration of interest

The authors declare no competing interests

Data availability

The data that support the findings of this study are available within the main text and its Supplementary Information file. The lead contact will share all raw data associated with this paper upon request. This study did not utilize or generate any unique datasets or codes.

462

463 ## References

464

465 1 Schieber, M. & Chandel, N. S. ROS function in redox signaling and oxidative stress. *Curr Biol*
466 **24**, R453-462, doi:10.1016/j.cub.2014.03.034 (2014).
467 2 Holmstrom, K. M. & Finkel, T. Cellular mechanisms and physiological consequences of redox-
468 dependent signalling. *Nat Rev Mol Cell Biol* **15**, 411-421, doi:10.1038/nrm3801 (2014).
469 3 D'Autreaux, B. & Toledano, M. B. ROS as signalling molecules: mechanisms that generate
470 specificity in ROS homeostasis. *Nat Rev Mol Cell Biol* **8**, 813-824, doi:10.1038/nrm2256 (2007).
471 4 Maryanovich, M. & Gross, A. A ROS rheostat for cell fate regulation. *Trends Cell Biol* **23**, 129-
472 134, doi:10.1016/j.tcb.2012.09.007 (2013).
473 5 Murphy, M. P. How mitochondria produce reactive oxygen species. *Biochem J* **417**, 1-13,
474 doi:10.1042/BJ20081386 (2009).
475 6 Hamanaka, R. B. & Chandel, N. S. Mitochondrial reactive oxygen species regulate cellular
476 signaling and dictate biological outcomes. *Trends Biochem Sci* **35**, 505-513,
477 doi:10.1016/j.tibs.2010.04.002 (2010).
478 7 Al-Mehdi, A. B. *et al.* Perinuclear mitochondrial clustering creates an oxidant-rich nuclear
479 domain required for hypoxia-induced transcription. *Sci Signal* **5**, ra47,
480 doi:10.1126/scisignal.2002712 (2012).
481 8 Bedard, K. & Krause, K. H. The NOX family of ROS-generating NADPH oxidases: physiology
482 and pathophysiology. *Physiol Rev* **87**, 245-313, doi:10.1152/physrev.00044.2005 (2007).
483 9 Appenzeller-Herzog, C. *et al.* Transit of H2O2 across the endoplasmic reticulum membrane is
484 not sluggish. *Free Radic Biol Med* **94**, 157-160, doi:10.1016/j.freeradbiomed.2016.02.030
485 (2016).
486 10 Mishina, N. M. *et al.* Which Antioxidant System Shapes Intracellular H(2)O(2) Gradients?
487 *Antioxid Redox Signal* **31**, 664-670, doi:10.1089/ars.2018.7697 (2019).
488 11 Yoboue, E. D., Sitia, R. & Simmen, T. Redox crosstalk at endoplasmic reticulum (ER)
489 membrane contact sites (MCS) uses toxic waste to deliver messages. *Cell Death Dis* **9**, 331,
490 doi:10.1038/s41419-017-0033-4 (2018).
491 12 Rehman, J. Empowering self-renewal and differentiation: the role of mitochondria in stem cells.
492 *J Mol Med (Berl)* **88**, 981-986, doi:10.1007/s00109-010-0678-2 (2010).
493 13 Li, T. S. & Marban, E. Physiological levels of reactive oxygen species are required to maintain
494 genomic stability in stem cells. *Stem Cells* **28**, 1178-1185, doi:10.1002/stem.438 (2010).
495 14 Le Belle, J. E. *et al.* Proliferative neural stem cells have high endogenous ROS levels that
496 regulate self-renewal and neurogenesis in a PI3K/Akt-dependant manner. *Cell Stem Cell* **8**, 59-
497 71, doi:10.1016/j.stem.2010.11.028 (2011).
498 15 Chuikov, S., Levi, B. P., Smith, M. L. & Morrison, S. J. Prdm16 promotes stem cell maintenance
499 in multiple tissues, partly by regulating oxidative stress. *Nat Cell Biol* **12**, 999-1006,
500 doi:10.1038/ncb2101 (2010).
501 16 Owusu-Ansah, E. & Banerjee, U. Reactive oxygen species prime Drosophila haematopoietic
502 progenitors for differentiation. *Nature* **461**, 537-541, doi:10.1038/nature08313 (2009).
503 17 Tan, S. W. S., Lee, Q. Y., Wong, B. S. E., Cai, Y. & Baeg, G. H. Redox Homeostasis Plays
504 Important Roles in the Maintenance of the Drosophila Testis Germline Stem Cells. *Stem Cell*
505 *Reports* **9**, 342-354, doi:10.1016/j.stemcr.2017.05.034 (2017).
506 18 Zhou, G., Meng, S., Li, Y., Ghebre, Y. T. & Cooke, J. P. Optimal ROS Signaling Is Critical for
507 Nuclear Reprogramming. *Cell Rep* **15**, 919-925, doi:10.1016/j.celrep.2016.03.084 (2016).
508 19 Morris, O. & Jasper, H. Reactive Oxygen Species in intestinal stem cell metabolism, fate and
509 function. *Free Radic Biol Med* **166**, 140-146, doi:10.1016/j.freeradbiomed.2021.02.015 (2021).
510 20 Sinenko, S. A., Shim, J. & Banerjee, U. Oxidative stress in the haematopoietic niche regulates
511 the cellular immune response in Drosophila. *EMBO Rep* **13**, 83-89,
512 doi:10.1038/embor.2011.223 (2011).
513 21 Davies, E. L. & Fuller, M. T. Regulation of self-renewal and differentiation in adult stem cell
514 lineages: lessons from the Drosophila male germ line. *Cold Spring Harb Symp Quant Biol* **73**,
515 137-145, doi:10.1101/sqb.2008.73.063 (2008).
516 22 Hime, G. R., Brill, J. A. & Fuller, M. T. Assembly of ring canals in the male germ line from
517 structural components of the contractile ring. *J Cell Sci* **109 (Pt 12)**, 2779-2788,
518 doi:10.1242/jcs.109.12.2779 (1996).

23 Gonczy, P. & DiNardo, S. The germ line regulates somatic cyst cell proliferation and fate during Drosophila spermatogenesis. *Development* **122**, 2437-2447, doi:10.1242/dev.122.8.2437 (1996).
24 Fabrizio, J. J., Boyle, M. & DiNardo, S. A somatic role for eyes absent (eya) and sine oculis (so) in Drosophila spermatocyte development. *Dev Biol* **258**, 117-128, doi:10.1016/s0012-1606(03)00127-1 (2003).
25 Hardy, R. W., Tokuyasu, K. T., Lindsley, D. L. & Garavito, M. The germinal proliferation center in the testis of Drosophila melanogaster. *J Ultrastruct Res* **69**, 180-190, doi:10.1016/s0022-5320(79)90108-4 (1979).
26 Chen, S., Lewallen, M. & Xie, T. Adhesion in the stem cell niche: biological roles and regulation. *Development* **140**, 255-265, doi:10.1242/dev.083139 (2013).
27 Inaba, M., Yuan, H., Salzmann, V., Fuller, M. T. & Yamashita, Y. M. E-cadherin is required for centrosome and spindle orientation in Drosophila male germline stem cells. *PLoS One* **5**, e12473, doi:10.1371/journal.pone.0012473 (2010).
28 Greenspan, L. J., de Cuevas, M. & Matunis, E. Genetics of gonadal stem cell renewal. *Annu Rev Cell Dev Biol* **31**, 291-315, doi:10.1146/annurev-cellbio-100913-013344 (2015).
29 Kiger, A. A., Jones, D. L., Schulz, C., Rogers, M. B. & Fuller, M. T. Stem cell self-renewal specified by JAK-STAT activation in response to a support cell cue. *Science* **294**, 2542-2545, doi:10.1126/science.1066707 (2001).
30 Tulina, N. & Matunis, E. Control of stem cell self-renewal in Drosophila spermatogenesis by JAK-STAT signaling. *Science* **294**, 2546-2549, doi:10.1126/science.1066700 (2001).
31 Kawase, E., Wong, M. D., Ding, B. C. & Xie, T. Gbb/Bmp signaling is essential for maintaining germline stem cells and for repressing bam transcription in the Drosophila testis. *Development* **131**, 1365-1375, doi:10.1242/dev.01025 (2004).
32 Michel, M., Kupinski, A. P., Raabe, I. & Bokel, C. Hh signalling is essential for somatic stem cell maintenance in the Drosophila testis niche. *Development* **139**, 2663-2669, doi:10.1242/dev.075242 (2012).
33 Song, X. *et al.* Bmp signals from niche cells directly repress transcription of a differentiation-promoting gene, bag of marbles, in germline stem cells in the Drosophila ovary. *Development* **131**, 1353-1364, doi:10.1242/dev.01026 (2004).
34 Losick, V. P., Morris, L. X., Fox, D. T. & Spradling, A. Drosophila stem cell niches: a decade of discovery suggests a unified view of stem cell regulation. *Dev Cell* **21**, 159-171, doi:10.1016/j.devcel.2011.06.018 (2011).
35 Jemc, J. C. Somatic gonadal cells: the supporting cast for the germline. *Genesis* **49**, 753-775, doi:10.1002/dvg.20784 (2011).
36 Zoller, R. & Schulz, C. The Drosophila cyst stem cell lineage: Partners behind the scenes? *Spermatogenesis* **2**, 145-157, doi:10.4161/spmg.21380 (2012).
37 Larsson, N. G. *et al.* Mitochondrial transcription factor A is necessary for mtDNA maintenance and embryogenesis in mice. *Nat Genet* **18**, 231-236, doi:10.1038/ng0398-231 (1998).
38 Sykiotis, G. P. & Bohmann, D. Keap1/Nrf2 signaling regulates oxidative stress tolerance and lifespan in Drosophila. *Dev Cell* **14**, 76-85, doi:10.1016/j.devcel.2007.12.002 (2008).
39 Fairchild, M. J., Yang, L., Goodwin, K. & Tanentzapf, G. Occluding Junctions Maintain Stem Cell Niche Homeostasis in the Fly Testes. *Curr Biol* **26**, 2492-2499, doi:10.1016/j.cub.2016.07.012 (2016).
40 Zielke, N. *et al.* Fly-FUCCI: A versatile tool for studying cell proliferation in complex tissues. *Cell Rep* **7**, 588-598, doi:10.1016/j.celrep.2014.03.020 (2014).
41 Ng, C. L., Qian, Y. & Schulz, C. Notch and Delta are required for survival of the germline stem cell lineage in testes of Drosophila melanogaster. *PLoS One* **14**, e0222471, doi:10.1371/journal.pone.0222471 (2019).
42 Amoyel, M., Hillion, K. H., Margolis, S. R. & Bach, E. A. Somatic stem cell differentiation is regulated by PI3K/Tor signaling in response to local cues. *Development* **143**, 3914-3925, doi:10.1242/dev.139782 (2016).
43 Castanieto, A., Johnston, M. J. & Nystul, T. G. EGFR signaling promotes self-renewal through the establishment of cell polarity in Drosophila follicle stem cells. *Elife* **3**, doi:10.7554/eLife.04437 (2014).
44 Papagiannouli, F., Berry, C. W. & Fuller, M. T. The Dlg Module and Clathrin-Mediated Endocytosis Regulate EGFR Signaling and Cyst Cell-Germline Coordination in the Drosophila Testis. *Stem Cell Reports* **12**, 1024-1040, doi:10.1016/j.stemcr.2019.03.008 (2019).
45 Chen, Y. & Struhl, G. Dual roles for patched in sequestering and transducing Hedgehog. *Cell* **87**, 553-563, doi:10.1016/s0092-8674(00)81374-4 (1996).

46 Chen, Y. & Struhl, G. In vivo evidence that Patched and Smoothened constitute distinct binding and transducing components of a Hedgehog receptor complex. *Development* **125**, 4943-4948, doi:10.1242/dev.125.24.4943 (1998).
47 Jiang, J. & Hui, C. C. Hedgehog signaling in development and cancer. *Dev Cell* **15**, 801-812, doi:10.1016/j.devcel.2008.11.010 (2008).
48 Sinenko, S. A., Starkova, T. Y., Kuzmin, A. A. & Tomilin, A. N. Physiological Signaling Functions of Reactive Oxygen Species in Stem Cells: From Flies to Man. *Front Cell Dev Biol* **9**, 714370, doi:10.3389/fcell.2021.714370 (2021).
49 Liang, R. & Ghaffari, S. Stem cells, redox signaling, and stem cell aging. *Antioxid Redox Signal* **20**, 1902-1916, doi:10.1089/ars.2013.5300 (2014).
50 Fu, X. J. *et al.* NADPH oxidase 1 and its derived reactive oxygen species mediated tissue injury and repair. *Oxid Med Cell Longev* **2014**, 282854, doi:10.1155/2014/282854 (2014).
51 Taylor-Fishwick, D. A. NOX, NOX Who is There? The Contribution of NADPH Oxidase One to Beta Cell Dysfunction. *Front Endocrinol (Lausanne)* **4**, 40, doi:10.3389/fendo.2013.00040 (2013).
52 Santabarbara-Ruiz, P. *et al.* Ask1 and Akt act synergistically to promote ROS-dependent regeneration in Drosophila. *PLoS Genet* **15**, e1007926, doi:10.1371/journal.pgen.1007926 (2019).
53 Bienert, G. P. *et al.* Specific aquaporins facilitate the diffusion of hydrogen peroxide across membranes. *J Biol Chem* **282**, 1183-1192, doi:10.1074/jbc.M603761200 (2007).
54 Milkovic, L., Cipak Gasparovic, A., Cindric, M., Mouthuy, P. A. & Zarkovic, N. Short Overview of ROS as Cell Function Regulators and Their Implications in Therapy Concepts. *Cells* **8**, doi:10.3390/cells8080793 (2019).
55 Pan, L. *et al.* Stem cell aging is controlled both intrinsically and extrinsically in the Drosophila ovary. *Cell Stem Cell* **1**, 458-469, doi:10.1016/j.stem.2007.09.010 (2007).
56 Leatherman, J. L. & Dinardo, S. Germline self-renewal requires cyst stem cells and stat regulates niche adhesion in Drosophila testes. *Nat Cell Biol* **12**, 806-811, doi:10.1038/ncb2086 (2010).
57 Bausek, N. JAK-STAT signaling in stem cells and their niches in Drosophila. *JAKSTAT* **2**, e25686, doi:10.4161/jkst.25686 (2013).
58 Gonczy, P., Matunis, E. & DiNardo, S. bag-of-marbles and benign gonial cell neoplasm act in the germline to restrict proliferation during Drosophila spermatogenesis. *Development* **124**, 4361-4371, doi:10.1242/dev.124.21.4361 (1997).
59 Butturini, E. *et al.* S-Glutathionylation at Cys328 and Cys542 impairs STAT3 phosphorylation. *ACS Chem Biol* **9**, 1885-1893, doi:10.1021/cb500407d (2014).
60 Xiong, Y., Uys, J. D., Tew, K. D. & Townsend, D. M. S-glutathionylation: from molecular mechanisms to health outcomes. *Antioxid Redox Signal* **15**, 233-270, doi:10.1089/ars.2010.3540 (2011).
61 Issigonis, M. *et al.* JAK-STAT signal inhibition regulates competition in the Drosophila testis stem cell niche. *Science* **326**, 153-156, doi:10.1126/science.1176817 (2009).
62 DeGennaro, M. *et al.* Peroxiredoxin stabilization of DE-cadherin promotes primordial germ cell adhesion. *Dev Cell* **20**, 233-243, doi:10.1016/j.devcel.2010.12.007 (2011).
63 Karsten, P., Hader, S. & Zeidler, M. P. Cloning and expression of Drosophila SOCS36E and its potential regulation by the JAK/STAT pathway. *Mech Dev* **117**, 343-346, doi:10.1016/s0925-4773(02)00216-2 (2002).
64 Richmond, C. A. *et al.* JAK/STAT-1 Signaling Is Required for Reserve Intestinal Stem Cell Activation during Intestinal Regeneration Following Acute Inflammation. *Stem Cell Reports* **10**, 17-26, doi:10.1016/j.stemcr.2017.11.015 (2018).
65 Kiger, A. A., White-Cooper, H. & Fuller, M. T. Somatic support cells restrict germline stem cell self-renewal and promote differentiation. *Nature* **407**, 750-754, doi:10.1038/35037606 (2000).
66 Schulz, C., Wood, C. G., Jones, D. L., Tazuke, S. I. & Fuller, M. T. Signaling from germ cells mediated by the rhomboid homolog stet organizes encapsulation by somatic support cells. *Development* **129**, 4523-4534, doi:10.1242/dev.129.19.4523 (2002).
67 Koundouros, N. & Poulogiannis, G. Phosphoinositide 3-Kinase/Akt Signaling and Redox Metabolism in Cancer. *Front Oncol* **8**, 160, doi:10.3389/fonc.2018.00160 (2018).
68 Senos Demarco, R. & Jones, D. L. Mitochondrial fission regulates germ cell differentiation by suppressing ROS-mediated activation of Epidermal Growth Factor Signaling in the Drosophila larval testis. *Sci Rep* **9**, 19695, doi:10.1038/s41598-019-55728-0 (2019).

637 69 Amoyel, M., Anderson, J., Suisse, A., Glasner, J. & Bach, E. A. Socs36E Controls Niche
638 Competition by Repressing MAPK Signaling in the Drosophila Testis. *PLoS Genet* **12**,
639 e1005815, doi:10.1371/journal.pgen.1005815 (2016).
640 70 Kalamakis, G. *et al.* Quiescence Modulates Stem Cell Maintenance and Regenerative Capacity
641 in the Aging Brain. *Cell* **176**, 1407-1419 e1414, doi:10.1016/j.cell.2019.01.040 (2019).
642 71 Snoeck, H. W. Can Metabolic Mechanisms of Stem Cell Maintenance Explain Aging and the
643 Immortal Germline? *Cell Stem Cell* **16**, 582-584, doi:10.1016/j.stem.2015.04.021 (2015).
644 72 Michel, M., Raabe, I., Kupinski, A. P., Perez-Palencia, R. & Bokel, C. Local BMP receptor
645 activation at adherens junctions in the Drosophila germline stem cell niche. *Nat Commun* **2**,
646 415, doi:10.1038/ncomms1426 (2011).

647

648

649 **Figure Legends**

650 **Figure 1. Mitochondrial Distribution and Redox Profile of GSCs and CySCs in**
651 **Adult *Drosophila* Testes**

652 (A) Schematic representation of adult *Drosophila* testicular niche showing
653 arrangement of different stem cell populations (GSC – Germinal Stem Cell, CySC –
654 Cyst Stem Cell). (B-E) Differential distribution of mitochondria labelled with ATP5A
655 (monochrome/green) in Vasa^{+} GSCs of wild-type fly testis with cellular boundaries
656 marked by Dlg; B# shows digitally zoomed image of the dotted area. (F) Quantification
657 of mitochondrial size per cell. Bars represent mean ± s.e.m., n = 10 fields of view; ****P*
658 *(unpaired t-test)<0.0001.* (G) Representation of mitochondrial shape,. that is circular
659 or elongated (less circular) in two stem cell populations. Bars represent mean ± s.e.m.,
660 n = 10 fields of view; ****P (unpaired t-test)<0.0001.* (H-Q) Redox profiling of testicular
661 stem cell niche using *gstD1*-GFP as intrinsic ROS reporter in control (H-L) and *Tj-Gal4*
662 driven *Sod1RNAi (Sod1i)* testis (M-Q). (R) Quantification of *gstD1*-GFP mean
663 fluorescence intensity (MFI) represented as fold change between GSCs and CySCs
664 in control. Data denotes mean ± s.e.m,, n = 25, ****P(unpaired t-test)<0.0001.* (S)
665 Quantification of cell-specific ROS content. Data denotes mean ± s.e.m, n = 25,
666 ****P(unpaired t-test)<0.0001.* Controls are the indicated driver line crossed with
667 *Oregon R*$^{+}$. Scale bar - 10 µm. See also Figure S1.

668

669 **Figure 2. Redox disequilibrium in Cyst stem cell lineage deregulates early**
670 **CySCs and decreases the GSC number**

671 (A-B) Distribution of Tj$^+$ CySC/early cyst cell around the hub (FasIII) in control and Tj
672 driven *Sod1RNAi* testis. (C-D) Represents the rosette arrangement of Vasa$^+$ GSCs
673 flanking the hub. The digitally magnified region around the hub (dotted line) as seen
674 in control (C#) and *Sod1RNAi* (D#). (E-G) Mean number of Tj$^+$ cells, Zfh1$^+$ early CySCs
675 and GSCs in control and *Sod1RNAi* lines shown as mean ± s.e.m, n = 10,
676 ****P(unpaired t-test)<0.0001, **P(unpaired t-test)<0.0001.* (H) Construct design of the
677 FUCCI reporter line for tracking the cell cycle stages in *Drosophila* tissues, containing
678 degrons of Cyclin B and E2F1 proteins fused with RFP or GFP. G1, S and G2/M is
679 represented by GFP$^+$, RFP$^+$ and dual labelled cells respectively. (I-J) Comparative
680 changes in the cell cycle phases (I) or Zfh1$^+$ cells (J) present in G1, S and G2/M phase
681 at the niche zone between control and *Tj>Sod1i*. Data denote mean ± s.e.m, n = 10,
682 ****P(unpaired t-test)<0.0001, **P(unpaired t-test)<0.001.* (K) Mean number of pH3+
683 cells, a mitotic marker. Data points denote mean ± s.e.m, n = 10. Scale bar - 10 µm.
684 See also Figure S2.

685

686 **Figure 3. ROS imbalance in CySCs promotes differentiation of both GSCs and**
687 **CySCs**

688 (A-D) Number of early CySCs (Zfh1$^+$) (A'- B'), late differentiating CCs (Eya$^+$) (A - B)
689 and Zfh1, Eya co-expressing population (A''- B'') were imaged, represented
690 schematically (C) and quantified with respect to control and *Sod1RNAi* lines (D). Data
691 points represent mean ± s.e.m, n = 10, ****P(unpaired t-test)<0.0001*. (E-F) The effect
692 of Sod1 depletion in CySCs on the differentiation status of GSCs as observed using
693 *Bam-GFP* reporter line. (G) The relative distance of the differentiation initiation zone
694 (Bam$^+$) from the hub (red) in control and *Sod1i* testis shown as mean ± s.e.m, n = 10,
695 ****P(unpaired t-test)<0.0001.* (H-J) The shape and size of the spectrosomes marked
696 with α-spectrin (green) were imaged (I''-J'') and quantified for their distance from the
697 hub (marked with asterisk) (H), n = 10, ****P(unpaired t-test)<0.0001*. Branched fusome
698 marks differentiating populations (I'-J'). (K-L) Comparative staining of CySC-GSC
699 contacts through adherens junction using E-cadherin (monochrome/green). Dotted
700 area near the hub has been expanded as inset to show loss of E-cadherin network.
701 (M) E-cadherin intensity histogram plot generated from ImageJ representing the mean
702 intensity of expression in the region flanking the hub and GSCs. (N-O) Fold change in

703 expression of Stat dependent transcripts Socs36E (N) and Ptp61F (O) among control
704 and *Sod1i* niche, obtained through qPCR. Data is shown as mean ± s.e.m, n = 3,
705 ****P(unpaired t-test)<0.0001*. ns – not significant. Scale bar - 10 µm. See also Figure
706 S3.

707

708 **Figure 4. Altered CySC redox state affects niche maintenance signals.**

709 (A-B) The expression of cell polarity marker Dlg (red) in control and *Sod1i* stem-cell
710 niche (A''-B''), (C-D) Representative image showing pErk distribution parallelly with Tj^+
711 cells and its expression pattern through Fire LUT (C''-D''). Scale bar - 10 µm. Mean
712 florescence intensity (MFI) corresponding to Dlg level (E) was quantified, n = 75,
713 ****P(unpaired t-test)<0.0001.* (F) MFI of total pErk expression was quantified, n =200,
714 ****P(unpaired t-test)<0.0001*. (G'-H') Representative image showing distribution of
715 Patched (Ptc) in Tj^+ cells in control and *Tj>Sod1i*. (I-J) Quantification of Ptc (I) and Hh
716 effector Ci (J) expression through fluorescence intensity as mean ± s.e.m, n (Ptc) =
717 90, n (Ci) = 200, ****P(unpaired t-test)<0.0001* (K-L) The number of $Vasa^+$ (K) and Tj^+
718 (L) cells across control, *Sod1i*, and *Sod1i/Hhi* rescue samples depicted as mean ±
719 s.e.m, n = 10, ****P(unpaired t-test)<0.0001*. See also Figure S4.

720

721 **Figure 5. Low CySC ROS sustains GSC maintenance**

722 (A-B) Bar graphs illustrating variations in $Vasa^+$ GSC (A) and Tj^+ CySCs (B) numbers
723 upon overexpressing Sod1 ($Tj>Sod^{OE}$), represented as mean ± s.e.m, n = 10,
724 ****P(unpaired t-test)<0.0001, *P(unpaired t-test)<0.01*. (C-E) The spectrosomes
725 labelled with α-spectrin (α-spec) were imaged (C'-D') and their number was quantified
726 (E), n = 10, ***P(unpaired t-test)<0.001*. (F-H) The initiation of gonialblast differentiation
727 was determined by measuring the distance of Bam^+ zone from hub (red), n = 10,
728 **P(unpaired t-test)<0.01* (F), (G''-H'') shows distribution of Bam^+ reporter expressing
729 cells. Scale bar - 10 µm. See also Figure S5.

730

731 **Figure 6. Proposed role of intercellular redox balance in germline maintenance**
732 **and differentiation**

GSC and CySC are associated with different mitochondria abundance which correspond to the presence of a redox differential between two stem cell populations. Disequilibrated redox potential among the two populations due to depletion of Superoxide dismutase, enhances CySC proliferation and precocious GSC differentiation, thereby disrupting the homeostatic balance between the two stem populations.

Figure 1

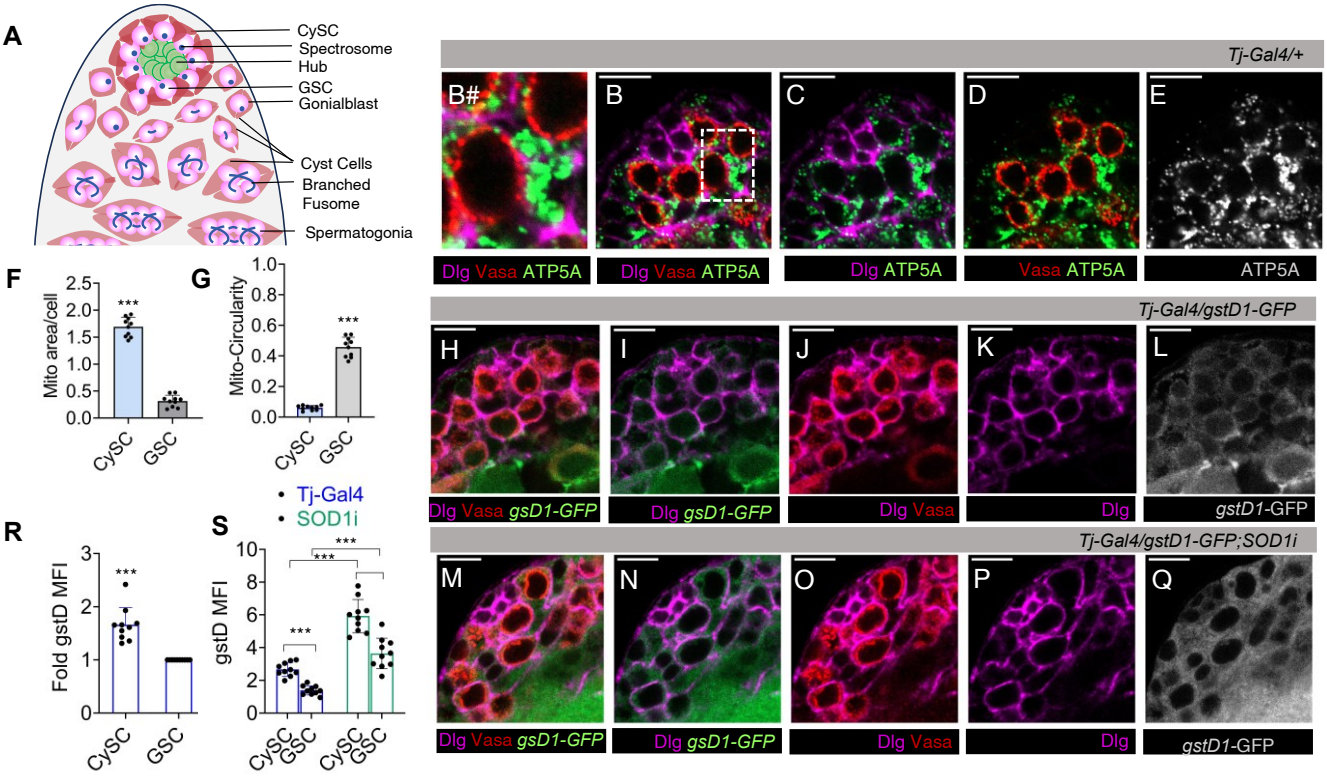
A
CySC
Spectrosome
Hub
GSC
Gonialblast
Cyst Cells
Branched Fusome
Spermatogonia
F
Mito area/cell
CySC
GSC
G
Mito-Circularity
CySC
GSC
R
Fold gstD MFI
CySC
GSC
S
Tj-Gal4
SOD1i
gstD MFI
CySC
GSC
CySC
GSC
Tj-Gal4/+
B#
B
C
D
E
Dlg Vasa ATP5A
Dlg Vasa ATP5A
Dlg ATP5A
Vasa ATP5A
ATP5A
Tj-Gal4/gstD1-GFP
H
I
J
K
L
Dlg Vasa gsD1-GFP
Dlg gsD1-GFP
Dlg Vasa
Dlg
gstD1-GFP
Tj-Gal4/gstD1-GFP;SOD1i
M
N
O
P
Q
Dlg Vasa gsD1-GFP
Dlg gsD1-GFP
Dlg Vasa
Dlg
gstD1-GFP

Figure 2

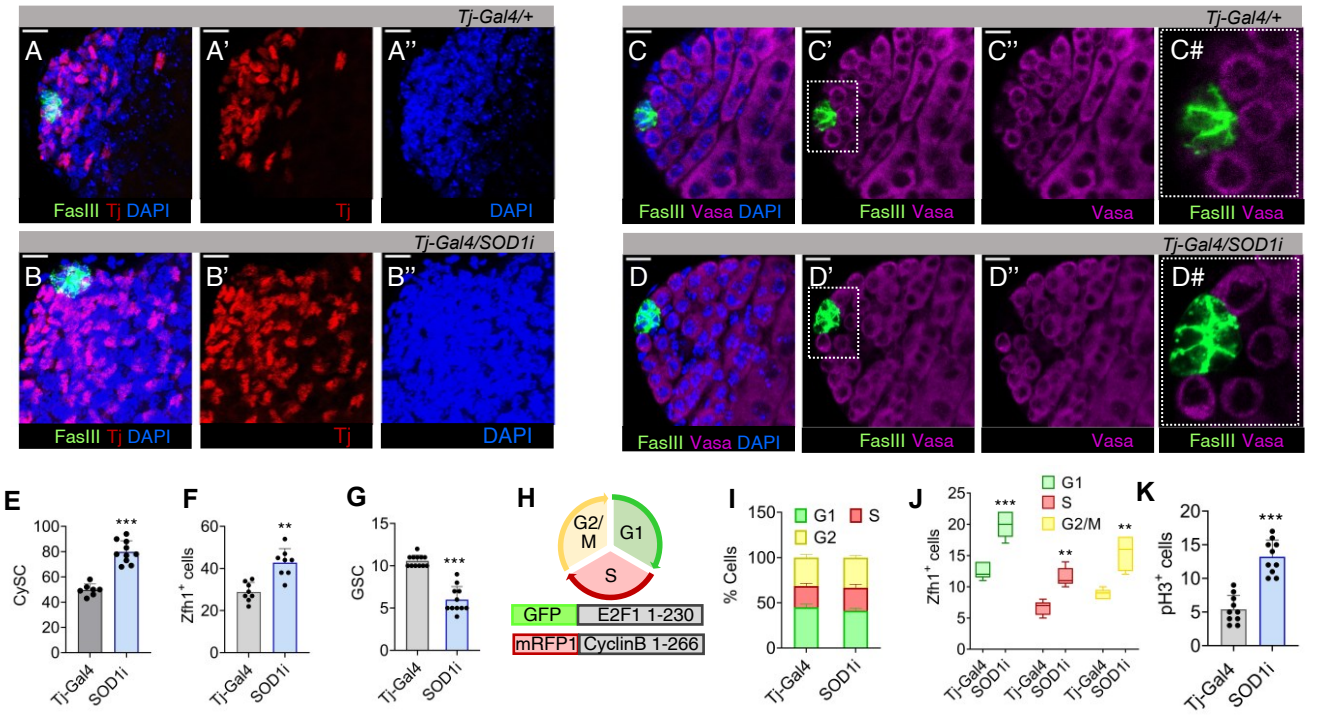
Tj-Gal4/+
A
A'
A''
FasIII Tj DAPI
Tj
DAPI
Tj-Gal4/SOD1i
B
B'
B''
FasIII Tj DAPI
Tj
DAPI
Tj-Gal4/+
C
C'
C''
C#
FasIII Vasa DAPI
FasIII Vasa
Vasa
FasIII Vasa
Tj-Gal4/SOD1i
D
D'
D''
D#
FasIII Vasa DAPI
FasIII Vasa
Vasa
FasIII Vasa
E
CySC
Tj-Gal4
SOD1i
F
Zfh1+ cells
G
GSC
H
G2/M
G1
S
GFP
E2F1 1-230
mRFP1
CyclinB 1-266
I
% Cells
G1
S
G2
J
Zfh1+ cells
G1
S
G2/M
K
pH3+ cells

Figure 3

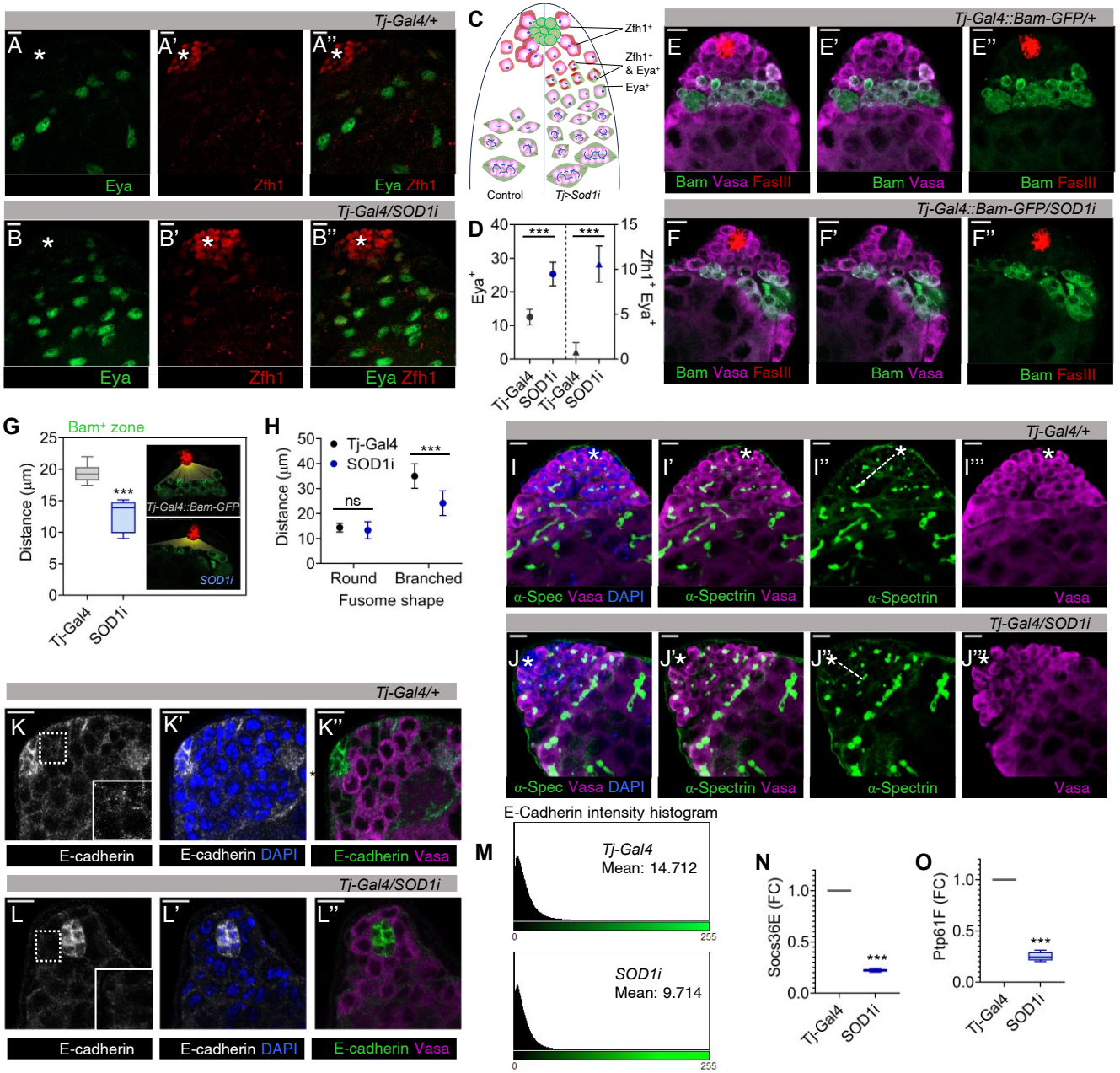
Tj-Gal4/+
A
A'
A''
Eya
Zfh1
Eya Zfh1
Tj-Gal4/SOD1i
B
B'
B''
Eya
Zfh1
Eya Zfh1
C
Zfh1+
Zfh1+ & Eya+
Eya+
Control
Tj>Sod1i
D
Eya+
Zfh1+ Eya+
***
***
Tj-Gal4
SOD1i
Tj-Gal4
SOD1i
Tj-Gal4::Bam-GFP/+
E
E'
E''
Bam Vasa FasIII
Bam Vasa
Bam FasIII
Tj-Gal4::Bam-GFP/SOD1i
F
F'
F''
Bam Vasa FasIII
Bam Vasa
Bam FasIII
G
Bam+ zone
Distance (µm)
***
Tj-Gal4::Bam-GFP
SOD1i
Tj-Gal4
SOD1i
H
Tj-Gal4
SOD1i
Distance (µm)
ns
***
Round
Branched
Fusome shape
Tj-Gal4/+
I
I'
I''
I'''
α-Spec Vasa DAPI
α-Spectrin Vasa
α-Spectrin
Vasa
Tj-Gal4/SOD1i
J
J'
J''
J'''
α-Spec Vasa DAPI
α-Spectrin Vasa
α-Spectrin
Vasa
Tj-Gal4/+
K
K'
K''
E-cadherin
E-cadherin DAPI
E-cadherin Vasa
Tj-Gal4/SOD1i
L
L'
L''
E-cadherin
E-cadherin DAPI
E-cadherin Vasa
E-Cadherin intensity histogram
M
Tj-Gal4
Mean: 14.712
SOD1i
Mean: 9.714
0
255
N
Socs36E (FC)
***
Tj-Gal4
SOD1i
O
Ptp61F (FC)
***
Tj-Gal4
SOD1i

Figure 4

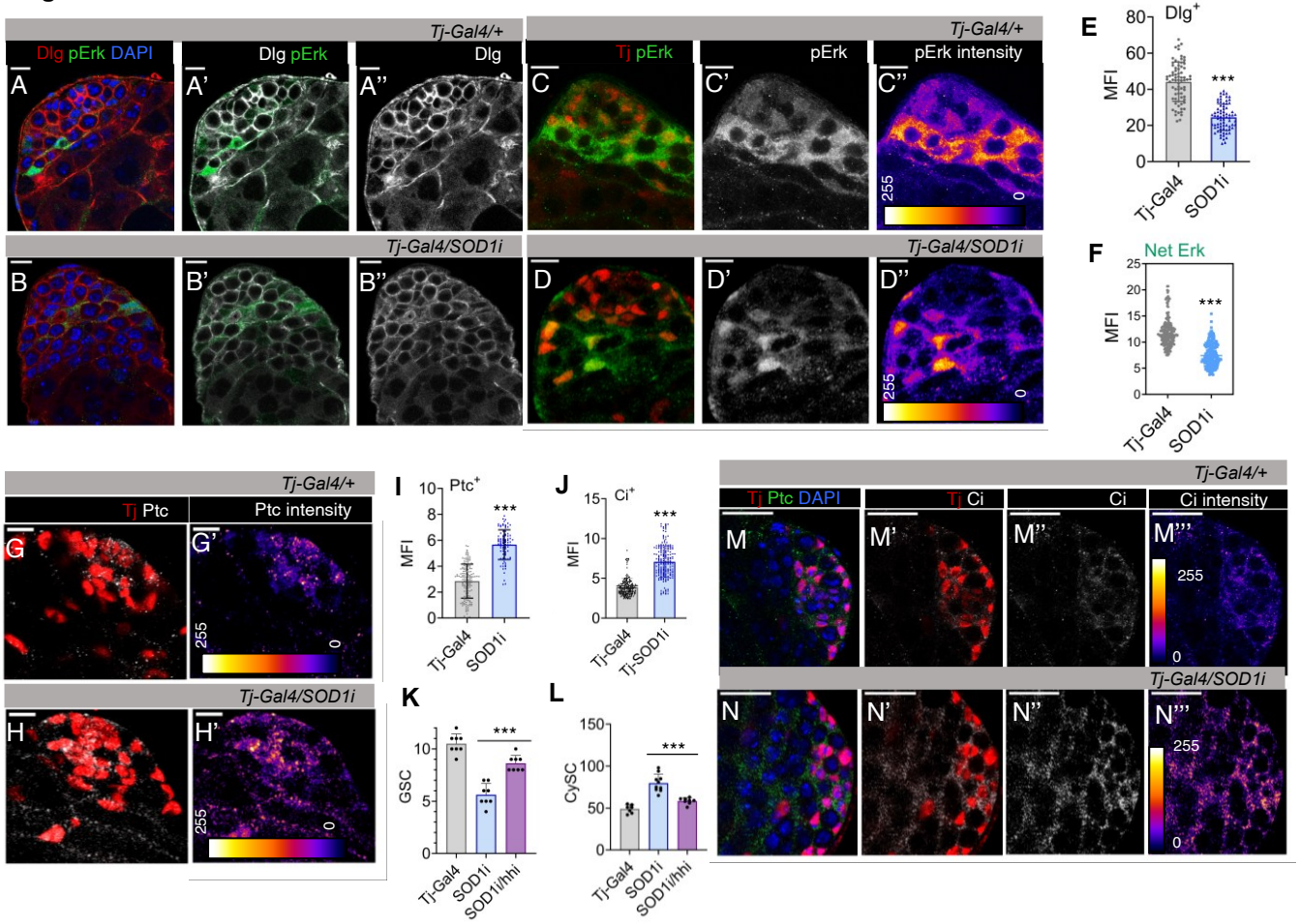
Tj-Gal4/+
Dlg pErk DAPI
Dlg pErk
Dlg
Tj pErk
pErk
pErk intensity
Tj-Gal4/SOD1i
A
A'
A''
B
B'
B''
C
C'
C''
D
D'
D''
255
0
E
Dlg+
MFI
***
Tj-Gal4
SOD1i
F
Net Erk
G
G'
Tj Ptc
Ptc intensity
H
H'
I
Ptc+
J
Ci+
K
GSC
SOD1i/hhi
L
CySC
M
M'
M''
M'''
Tj Ptc DAPI
Tj Ci
Ci
Ci intensity
N
N'
N''
N'''

Figure 5

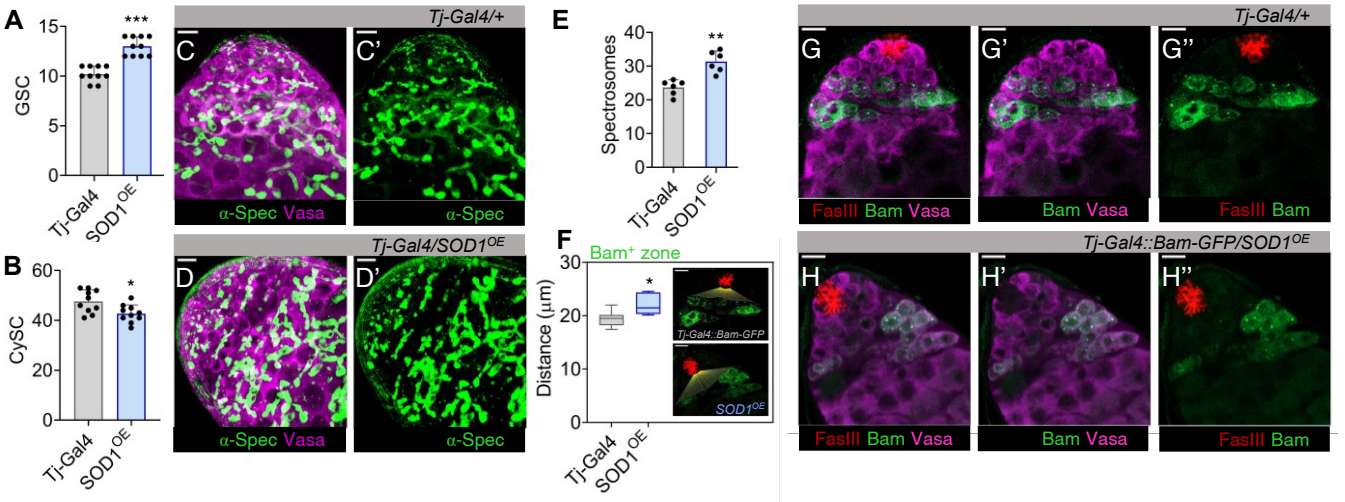
A
GSC
15
10
5
0
***
Tj-Gal4
SOD1 OE
B
CySC
60
40
20
0
*
Tj-Gal4
SOD1 OE
Tj-Gal4/+
C
C'
α-Spec Vasa
α-Spec
Tj-Gal4/SOD1OE
D
D'
α-Spec Vasa
α-Spec
E
Spectrosomes
40
30
20
10
0
**
Tj-Gal4
SOD1 OE
F
Bam+ zone
Distance (μm)
30
20
10
0
*
Tj-Gal4
SOD1 OE
Tj-Gal4::Bam-GFP
SOD1OE
Tj-Gal4/+
G
G'
G''
FasIII Bam Vasa
Bam Vasa
FasIII Bam
Tj-Gal4::Bam-GFP/SOD1OE
H
H'
H''
FasIII Bam Vasa
Bam Vasa
FasIII Bam

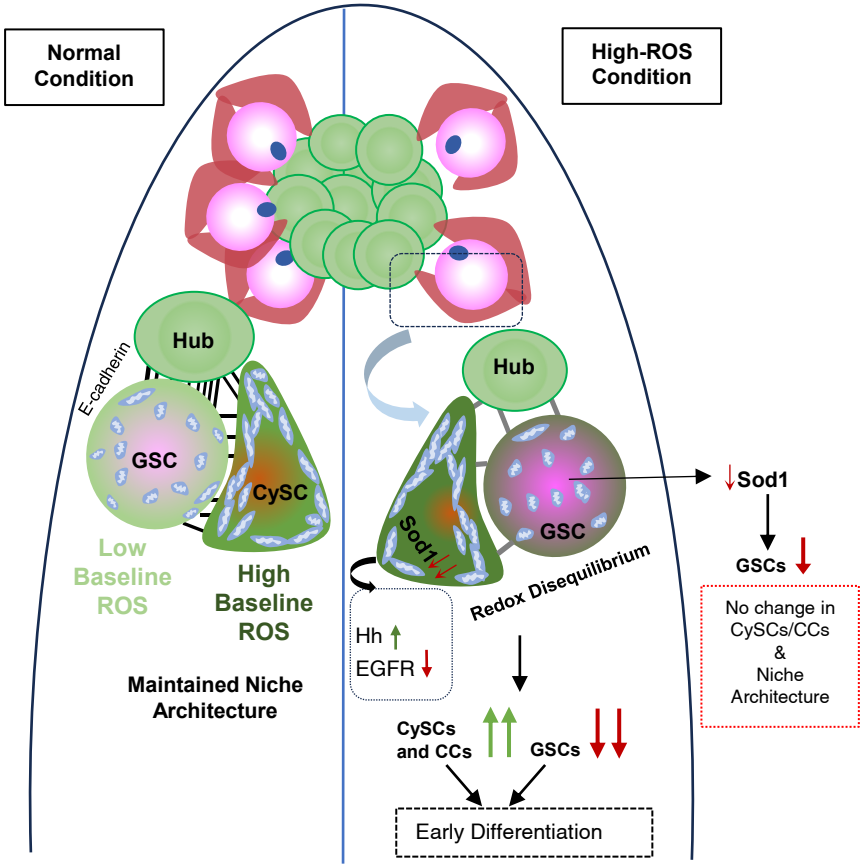
Normal Condition
High-ROS Condition
Hub
E-cadherin
GSC
CySC
Low Baseline ROS
High Baseline ROS
Maintained Niche Architecture
Hub
Sod1
GSC
Redox Disequilibrium
Hh
EGFR
CySCs and CCs
GSCs
Early Differentiation
Sod1
GSCs
No change in CySCs/CCs & Niche Architecture